nature physics

ARTICLES

PUBLISHED ONLINE: 19 SEPTEMBER 2016 | DOI: 10.1038/NPHYS3877

Controlled finite momentum pairing and spatially varying order parameter in proximitized HgTe quantum wells

Sean Hart[1†], Hechen Ren[1†], Michael Kosowsky[1], Gilad Ben-Shach[1], Philipp Leubner[2], Christoph Brüne[2], Hartmut Buhmann[2], Laurens W. Molenkamp[2], Bertrand I. Halperin[1] and Amir Yacoby[1*]

Conventional *s*-wave superconductivity arises from singlet pairing of electrons with opposite Fermi momenta, forming Cooper pairs with zero net momentum. Recent studies have focused on coupling *s*-wave superconductors to systems with an unusual configuration of electronic spin and momentum at the Fermi surface, where the nature of the paired state can be modified and the system may even undergo a topological phase transition. Here we present measurements and theoretical calculations of HgTe quantum wells coupled to aluminium or niobium superconductors and subject to a magnetic field in the plane of the quantum well. We find that this magnetic field tunes the momentum of Cooper pairs in the quantum well, directly reflecting the response of the spin-dependent Fermi surfaces. In the high electron density regime, the induced superconductivity evolves with electron density in agreement with our model based on the Hamiltonian of Bernevig, Hughes and Zhang. This agreement provides a quantitative value for $\tilde{g}/v_F$, where $\tilde{g}$ is the effective *g*-factor and v_F is the Fermi velocity. Our new understanding of the interplay between spin physics and superconductivity introduces a way to spatially engineer the order parameter from singlet to triplet pairing, and in general allows investigation of electronic spin texture at the Fermi surface of materials.

Below a critical temperature and magnetic field, certain materials undergo a phase transition to the superconducting state. Macroscopically identified through effects such as zero resistivity and the Meissner effect[1], superconductors may further be understood microscopically as arising due to pairing of electrons occupying opposite points on the Fermi surface and having opposite spin[2]. Within a conventional setting this interaction results in Cooper pairs with zero net momentum. However, in certain materials the presence of both magnetic order and superconductivity can lead to intrinsically non-zero pairing momentum as the system enters the Fulde–Ferrell–Larkin–Ovchinnikov state[3,4]. Studies of both $CeCoIn_5$ and κ-$(BEDT\text{-}TTF)_2Cu(NCS)_2$ under large external magnetic fields found evidence for coupled magnetic order and superconductivity, although in each material the field strength needed was in excess of 10 T (refs 5,6).

Exotic superconductivity has recently come under additional investigation through the goal of combining *s*-wave superconductors with materials whose properties are rarely found among the conventional superconductors. For example, inducing pairing from an *s*-wave superconductor into a material with strong spin–orbit coupling and reduced dimensionality has been recently considered as a viable platform within which to achieve triplet pairing[7,8] and topological superconductivity[9,10], or to engineer a Josephson ϕ_0-junction[11,12]. Moreover, when a ferromagnetic layer is sandwiched by two superconductors, pairs traversing the junction acquire momentum due to the exchange field within the ferromagnet[13,14]. Measurements of critical current oscillations in such superconductor–ferromagnet–superconductor junctions have provided evidence for both π-junctions and non-zero pairing momentum[15–18].

Here we report on coupling between superconducting leads and a two-dimensional electron system realized within HgTe/HgCdTe heterostructures in the inverted regime. Due to the interplay between superconductivity, band structure, and the applied magnetic field, we find that the order parameter has an oscillatory component derived from the finite momentum of paired electrons, and that this momentum can be continuously tuned between conventional and unconventional regimes. Our use of only relatively small external magnetic fields ($\lesssim$4 T) and micrometre-scale device dimensions introduces a new regime in the exploration of the interplay between superconductivity and spin physics.

To study the effect of magnetic field and band structure on electron pairing, we place two superconducting leads on opposite boundaries of a rectangular section of quantum well. Devices were fabricated at varying angles with respect to the cleavage edges of the crystal (the [110] and [1$\bar{1}$0] axes). The angular alignment corresponds to a rotation angle θ with respect to the principal crystal axis [100], with θ defined modulo $\pi/2$ (Fig. 1a, see Supplementary Information I). The width W between the two leads is 800 nm and the length L of the resulting Josephson junction is 4 μm. We study the influence of either niobium or aluminium superconductors by applying a small a.c current bias between the two leads while measuring the resultant a.c. voltage[19]. The aluminium thickness is 15 nm in order to sustain superconductivity in moderate parallel magnetic fields (Supplementary Information II)[20], while the niobium thickness is 130 nm. Josephson interference is generated by application of small (up to ∼10 mT) magnetic fields in the z direction[21]. Throughout, the in-plane coordinate axes are referred to as x and y, respectively oriented perpendicular and parallel to

[1]Department of Physics, Harvard University, Cambridge, Massachusetts 02138, USA. [2]Physikalisches Institut (EP3), Universität Würzburg, 97074 Würzburg, Germany. †These authors contributed equally to this work. *e-mail: yacoby@physics.harvard.edu

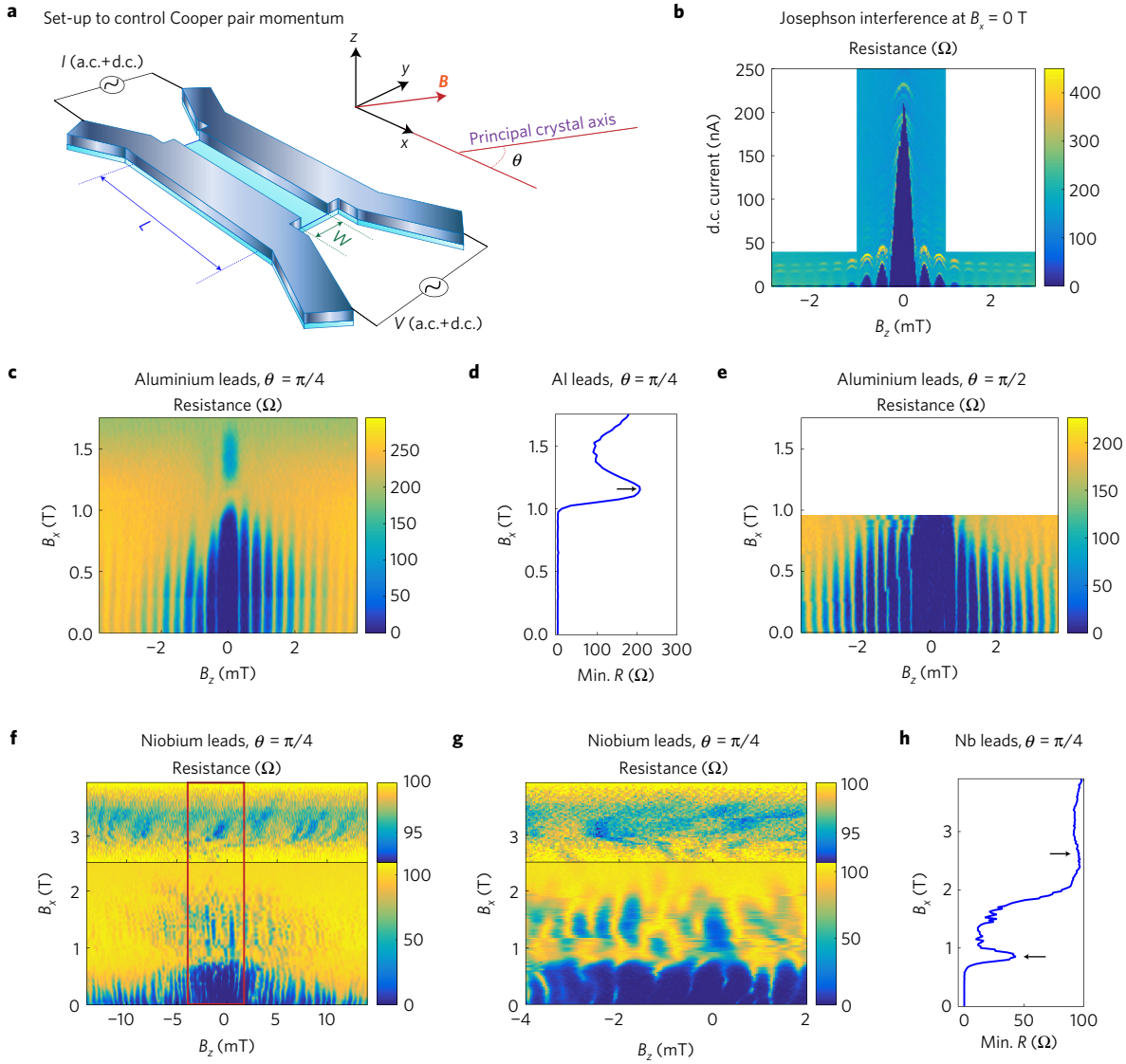

Figure 1 | Experimental control of the order parameter and of pairing momentum. a, Two superconducting leads, composed of either aluminium or niobium, couple to a rectangular section of HgTe quantum well to form a Josephson junction. The width W separating the leads is always 800 nm, while the length L of the junction is always 4 μm. The resistance of the junction is monitored by applying a small a.c. current bias (typically ∼1 nA) and concurrently measuring the resulting a.c. voltage. Further sourcing d.c. current allows measurement of critical currents and normal device resistance. The external magnetic field $\boldsymbol{B}$ contains a small z component to generate Josephson interference, while here the larger x component couples significantly to the spin degree of freedom. Junctions may be oriented at an angle θ with respect to the [100] principal crystal axis, modulo $\pi/2$. **b**, In the electron-doped regime, the devices show Josephson interference consistent with transport through a doped bulk. In all subsequent measurements, zero d.c. current is applied. **c**, The differential resistance of a junction with aluminium leads oscillates due to Josephson interference as the perpendicular field varies. Increasing the parallel field modulates the strength of induced superconductivity. **d**, Plotting the minimum resistance at each value of B_x demonstrates the presence of a nodal resistance maximum near $B_x = 1.1$ T. **e**, In an aluminium-based device oriented with $\theta = \pi/2$, increasing the parallel field similarly modifies the resistance. **f**, In a junction with niobium leads, a similar modulation of the resistance occurs. **g**, A more detailed study of the space outlined in red in **f** highlights three regions of decreased resistance separated by bands of high resistance near $B_x = 0.9$ T and $B_x = 2.7$ T. In both **f** and **g**, the decreased resistance above 2.5 T is highlighted via a stretched colour scale. **h**, The minimum resistance at each value of B_x further shows the oscillatory nature of the superconductivity as the parallel field increases. Successively higher nodes (marked by arrows) occupy broader regions of parallel field, while superconductivity also weakens as the parallel field increases.

the supercurrent flow between leads. The addition of a normal metal topgate allows us to study superconductivity over a range of density in the electron-doped regime. Previous experiments have also investigated the behaviour of devices as the electron density is further depleted into the quantum spin Hall regime[22,23]. In the regime of high electron density and with no parallel magnetic field, our junctions display Josephson interference consistent with uniform supercurrent transport through the bulk of the quantum well, shown in Fig. 1b for a device with aluminium leads.

We primarily study differential resistance with zero applied d.c current, due to the efficiency of such measurements in illuminating the structure of the interference pattern. Lower resistance relative to the normal device resistance typically corresponds to elevated critical current (Supplementary Information III). In an aluminium-based junction, with the topgate voltage set to 0.5 V and with angle $\theta = \pi/4$, increasing the magnetic field in the x direction strongly modulates the Josephson interference (Fig. 1c). Two distinct regions of decreased resistance are separated by a nodal

field of approximately $B_x = 1.1$ T, corresponding to the suppression of induced superconductivity. At each value of the parallel field, we extract the minimum junction resistance as a measure of the strength of superconductivity at that particular field. Plotting these minimum junction resistances highlights the oscillatory effect of parallel field on superconductivity, with the nodal field marked by an arrow (Fig. 1d). The suppression of superconductivity at the nodal field directly results from the finite momentum of induced Cooper pairs.

In an aluminium-based junction, with the topgate set to 0 V and oriented with $\theta = \pi/2$, a similar modulation of superconductivity occurs as the parallel field B_x grows (Fig. 1e, see Supplementary Information IV–V). Although the aluminium leads can sustain superconductivity up to 1.75 T, we measure this device only up to $B_x = 1$ T due to constraints on the range of our vector magnet (see Supplementary Information I).

The resistance of a device with niobium leads and $\theta = \pi/4$ is similarly modulated following application of a parallel field, with multiple nodes visible as B_x increases to 4 T (Fig. 1f). For these measurements the topgate voltage was set to 0 V. A more detailed measurement highlights the presence of three distinct regions of decreased resistance, separated by bands of high resistance occurring near $B_x = 0.9$ T and $B_x = 2.7$ T (Fig. 1g). We again extract the minimum junction resistance at each particular parallel field value, demonstrating the oscillatory effect of parallel field on superconductivity (Fig. 1h). Nodes of the oscillation, marked by arrows, correspond to local maxima in the overall junction resistance.

Despite the differences in fabrication of our devices, the nodal structure is both robust and occurs at nearly the same parallel field magnitudes. These observations suggest that the induced pairing momentum originates in the heterostructures and not the bulk superconductors, and is insensitive to details of the crystal orientation. Since superconductivity arises from pairing of electrons with opposing spins and momenta, it is therefore necessary to examine the nature of both Zeeman coupling and spin–orbit coupling within the quantum well.

We model our devices by considering first the quantum well region in the absence of the superconductors, for which a four-band theoretical Hamiltonian H_1 was proposed as a way to describe the topology of the band structure[24]. We adopt a version of this model to include both the external magnetic field and possible contributions from spin–orbit coupling[25–27]. The key prediction of the band structure modelling is that the Zeeman coupling from the external field B_x modifies the Fermi surfaces in a manner that depends on the nature of the spin–orbit coupling (Supplementary Information VI). As a consequence, the induced superconducting order parameter is expected to oscillate in space, due to a pairing momentum shift with magnitude of order $\hbar\Delta k \approx \tilde{g}\mu_B B_x/v_F$, whose orientation also depends on the spin–orbit coupling. Here $\tilde{g}$ is the in-plane g-factor, and v_F is the Fermi velocity.

To theoretically investigate the proximity effect in our quantum wells, we consider a model in which the two-dimensional electron gas (2DEG), assumed to have uniform electron density, is contacted by a pair of superconducting leads with a controlled phase difference between them, and we seek to calculate the maximum supercurrent that can be carried between the strips (see Supplementary Information VII–X for details not presented in the main text). Our model calculations cannot predict the absolute value of the critical current, but they should give the correct dependence on parameters such as the strength and direction of the magnetic field. We assume a Hamiltonian $H = H_1 + H_2$, where H_2 is the coupling between the superconductors and the 2DEG, described by a pairing Hamiltonian of the form

$$H_2 = -\int \mathrm{d}x\mathrm{d}y \left[\Delta\left(x,y\right)\Psi^{\dagger}\left(x,y\right) + \Delta^{*}\left(x,y\right)\Psi\left(x,y\right)\right] \quad (1)$$

Here $\Psi\left(x,y\right) \equiv \psi_{\uparrow}(x,y)\psi_{\downarrow}(x,y)$ is an operator that annihilates a singlet pair of electrons in the 2DEG at the point (x,y), while the pair potential $\Delta(x,y)$ is a complex number that depends on the phase of the superconductor and the tunnelling amplitude at that point.

We assume that the contacts between the 2DEG and the superconductors occur at the edges of the superconductors, located at $y = 0$ and $y = W$, so that we may write

$$\begin{aligned}\Delta\left(x,y\right) &= \lambda_1(x)\,\delta\left(y\right) + \lambda_2(x)\,\delta\left(y-W\right)\\ &\equiv \Delta_1\left(x,y\right) + \Delta_2(x,y)\end{aligned} \quad (2)$$

with $-L/2 < x < L/2$. We assume that the magnitude of the coupling is constant along each lead, but the phase will vary if there is a perpendicular magnetic field $B_z \neq 0$. We choose a gauge where the vector potential points in the x direction, with $A_x = -B_z(y - W/2)$, so that the vector potential vanishes along the midline of the 2DEG. If the superconducting strips have identical widths W_{SC}, then the couplings λ_j will have the form

$$\lambda_j(x) = \left|\lambda_j\right| \mathrm{e}^{2\pi i\phi_j(x)} \quad (3)$$

$$\phi_j(x) = \phi_j(0) + \frac{(-1)^{j-1} x B_z (W + W_{SC})}{2\Phi_0} \quad (4)$$

with $j = 1, 2$.

To lowest order in the couplings λ_j, the portion of the total energy that depends on the phase difference between the two superconducting leads can be written in the form:

$$E = -\int \mathrm{d}x_2 \left[\lambda_2^{*}(x_2)\left\langle\Psi(x_2,W)\right\rangle_1 + c.c.\right] \quad (5)$$

where $\langle\Psi(x,y)\rangle_1$ is the order parameter at point (x,y) induced by the superconductor $j = 1$. In turn, this may be written in the form

$$\left\langle\Psi(x,y)\right\rangle_1 = \int \mathrm{d}x_1 \lambda_1(x_1) F(x,x_1,y) \quad (6)$$

where F is the propagator from point $(x_1, 0)$ to point (x,y) for an induced Cooper pair. Depending on the relative magnitudes of spin–orbit coupling and the Zeeman coupling, the propagator F may take various forms (see Supplementary Information IX). Here we consider both structural inversion asymmetry (SIA), referring to asymmetry of the quantum well in the z direction[28], and bulk inversion asymmetry (BIA), referring to inversion asymmetry of the underlying crystal lattice[29]. In the limit where either SIA or BIA is strong compared with the Zeeman coupling, the pair momentum shift orientation is independent of position on the Fermi surface. The shift occurs along an angle α with respect to the x axis, and the propagator is

$$\begin{aligned}F\left(x,x_1,y\right) &= \frac{k_F}{8\pi^2 v_F}\cdot\frac{\mathrm{e}^{i\gamma} + \mathrm{e}^{-i\gamma}}{\left(x-x_1\right)^2 + y^2}\\ \gamma &= \Delta k\left(\sin(\alpha)y + \cos(\alpha)(x-x_1)\right)\end{aligned} \quad (7)$$

In Fig. 2, we calculate the order parameter $\langle\Psi(x,y)\rangle_1$ for several different limiting cases. When SIA dominates the spin–orbit coupling, a magnetic field B_x induces pairing momentum in the y direction, and the order parameter also oscillates in the y direction (Fig. 2a). When $\Delta kW = \pi/2$, the first node of the oscillation coincides with the line $y = W$ corresponding to the width of the junction. Increasing the parallel field so that $\Delta kW = 3\pi/2$ leads to coincidence of the second node and the junction width (Fig. 2b).

If BIA instead dominates the spin–orbit coupling, when $\theta = 0$ the parallel magnetic field induces order parameter oscillations in

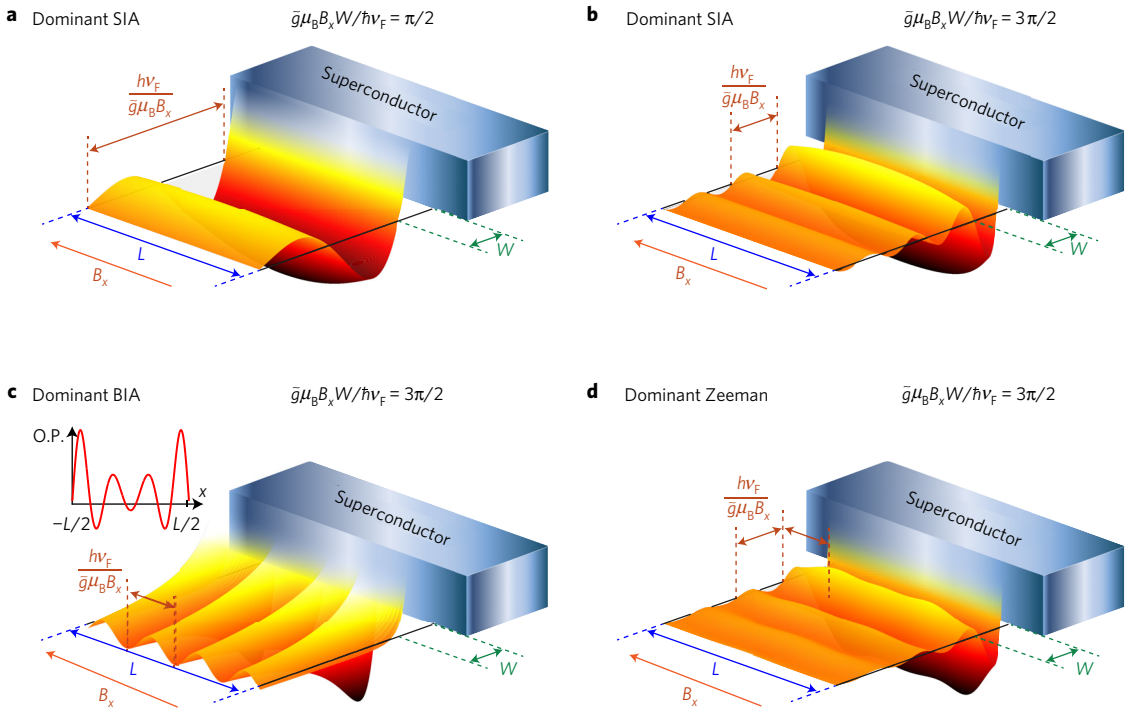

Figure 2 | Theoretical prediction for the spatially varying order parameter $\langle\Psi(x,y)\rangle_1$ near a single superconducting lead, with $B_z = 0$. a, With dominant SIA, application of an in-plane magnetic field B_x induces oscillations of the order parameter in the y direction, with wavelength $hv_F/\tilde{g}\mu_B B_x$. When $\tilde{g}\mu_B B_x W/\hbar v_F = \pi/2$ the first node of the order parameter occurs a distance W from the superconductor. **b**, As the magnitude of magnetic field increases, the wavelength of order parameter oscillations decreases. When $\tilde{g}\mu_B B_x W/\hbar v_F = 3\pi/2$, the second order parameter node lies a distance W from the superconductor. **c**, If instead BIA dominates, the order parameter oscillations occur in the x direction. As the magnetic field increases, the frequency of oscillations increases. In the inset, a linecut of the order parameter a distance W from the superconductor demonstrates that oscillations are an end effect, with amplitudes that decay into the bulk of the 2DEG. **d**, With weak spin–orbit coupling, the parallel field B_x introduces order parameter oscillations in both directions.

the x direction (Fig. 2c). These oscillations arise due to the finite length of the Josephson junction, with amplitudes that are largest near the ends of the mesa. In contrast to the limit of large SIA, with dominant BIA the nodes of the order parameter never coincide with the junction width. Oscillations in the order parameter instead occur with greater frequency along the x direction as the magnetic field increases.

Finally, when the Zeeman coupling dominates the spin–orbit coupling, the pair momentum shift magnitude is isotropic in-plane, but the orientation lies parallel to the direction of Cooper pair propagation. In this limit the propagator is

$$F(x,x_1,y) = \frac{k_F}{8\pi^2 v_F} \cdot \frac{e^{i\gamma} + e^{-i\gamma}}{(x-x_1)^2 + y^2}, \gamma = \Delta k\sqrt{(x-x_1)^2 + y^2} \quad (8)$$

Here the induced order parameter oscillates along both the x and y directions (Fig. 2d). Although the shape of the order parameter resembles the limit of strong SIA, the possibility to oscillate in all in-plane directions prevents a node from forming along a line of constant y.

We can link the order parameter oscillations to the Josephson energy E by integrating over the second superconducting lead at position $y = W$, as in equation (5). By then differentiating with respect to the phase difference $\phi_2(0) - \phi_1(0)$ we find the current-phase relation of the junction, which is then maximized with respect to the phase difference to obtain the critical current (Fig. 3a).

When SIA dominates the spin–orbit coupling, the critical current periodically disappears when the nodal condition $\Delta kW = (2n+1)\pi/2$ is satisfied (Fig. 3b). This suppression of the critical current arises when singlet pairs injected at one lead evolve to become triplet pairs at the location of the second lead. The conversion to triplet pairing corresponds to nodes of the induced singlet order parameter; when these nodes coincide with the positions of the leads, the supercurrent is completely suppressed. Microscopically, these oscillations of the order parameter correspond to finite momentum pairing of electrons, as diagrammed in the inset of Fig. 3b. In the limit of strong SIA, the Fermi surfaces oppositely shift in the y direction, so that Cooper pairs form internally to each surface with finite wavevector $\Delta k\hat{y}$. Furthermore, as the parallel magnetic field B_x increases beyond the nodal field $B_{node} = (\pi/2)\cdot(\hbar v_F/\tilde{g}\mu_B W)$, we observe evidence that the junction transitions into a π-junction (Supplementary Information XII).

The predicted interference with strong SIA resembles the nodal pattern we observe experimentally, and this good agreement suggests that our junctions are in the ballistic regime. However, in both aluminium- and niobium-based devices we also observe that superconductivity weakens as the parallel field increases, in contrast with the cosine dependence predicted by our model. We believe that this effect results from spatially inhomogeneous screening of the parallel field at the edges of the superconducting leads. The superconductor repels the in-plane field and slight roughness at the edges results in a weak magnetic field along the z direction that is positive at some locations and negative at others. This screening leads to a spatially varying random component of the phase that grows linearly with the in-plane field. Hence, we introduce a random phase $\chi \propto (R_1(x_1) - R_2(x_2))B_x$, where the random variables $R_1(x_1)$ and $R_2(x_2)$ correspond to screening of the parallel field at each interface (see Supplementary Information XI for details). With this randomness, the calculated critical currents diminish in magnitude as the in-plane field increases, in agreement with our experimental observation (Fig. 3c).

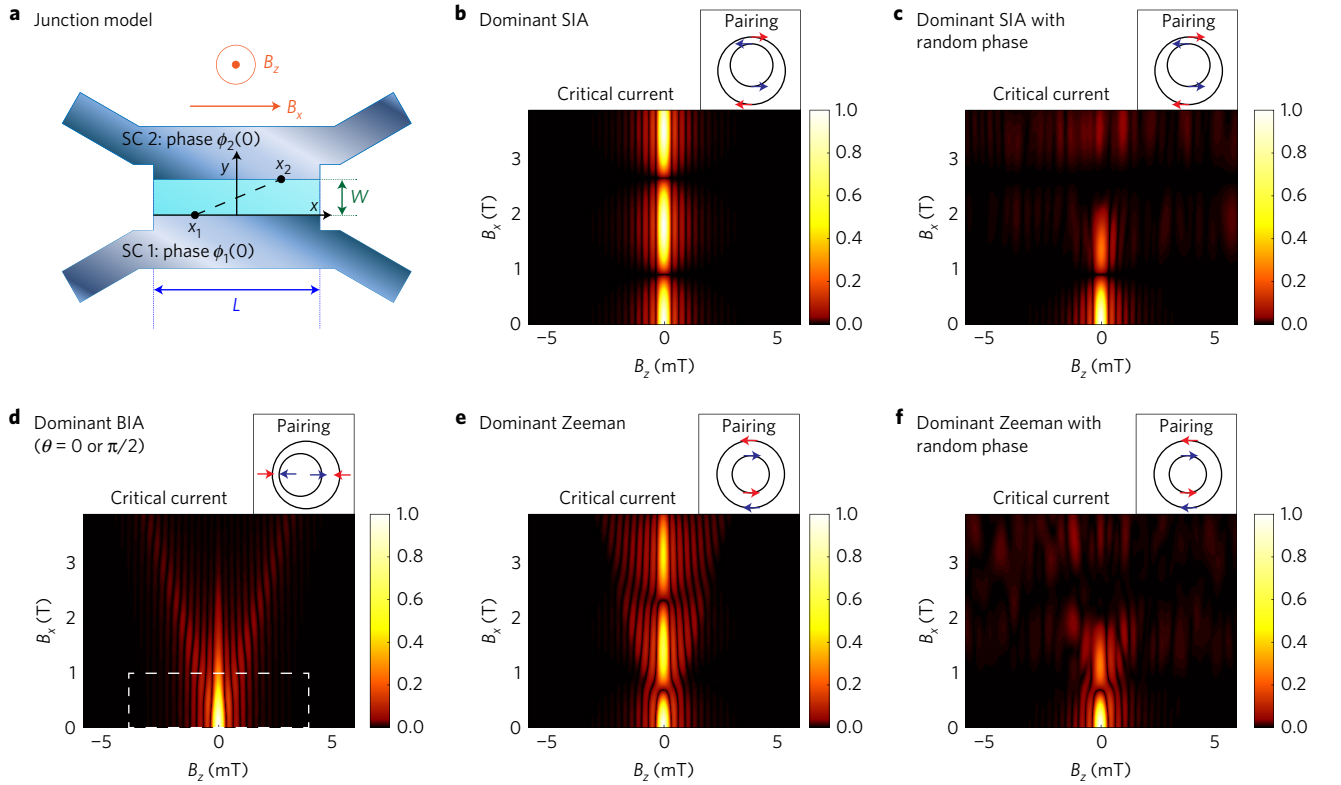

Figure 3 | Modelling Josephson interference between two superconducting leads. a, With two leads, paired electrons may traverse the junction beginning at a point x_1 in the lower superconducting lead (SC 1). The pairing amplitude at the point x_2 in the upper lead (SC 2) takes account of the phase accumulated due to finite pairing momentum within the HgTe quantum well. **b**, With SIA dominant, the external magnetic field B_x increases the pairing wavevector Δk only in the y direction. At certain values $\Delta k = (2n+1)\pi/(2W)$, where n is an integer, the superconducting interference disappears. A diagram schematically depicts the expected Fermi surfaces and Cooper pairing, where arrows denote spin direction and pairs are each coloured blue or red. Similar diagrams throughout this figure indicate the expectation for pairing and Fermi surfaces as the model parameters change. **c**, Randomness at the interface between the quantum well and superconductors may arise due to structural imperfections. The random phase causes superconductivity to weaken as the parallel field increases. **d**, For junctions aligned to a principal crystal axis, dominant BIA leads to a pairing wavevector Δk that grows in the x direction as B_x increases. The critical current maxima then occur at increasingly large values of $|B_z|$ as B_x grows. Fabricating devices at varying angles with respect to the crystal is expected to modify the interference when BIA dominates. The region outlined in dashed white corresponds to the measured region in Fig. 1e. **e**, With dominant Zeeman coupling, the pairing magnitude is isotropic in-plane and the interference grows as a hybrid of the SIA and BIA cases. Characteristically, interference fringes repeatedly combine to form the central fringe at each successive node in the parallel field. Additionally, with zero perpendicular field, superconductivity disappears at values of parallel field that are smaller than the nodal magnetic field in the case with dominant SIA. **f**, Including randomness leads to a similar picture to **c**, while retaining the combining of fringes characteristic of dominant Zeeman coupling.

Considering, instead, BIA as the dominant source of spin–orbit coupling, when the junction is aligned to the [100] or [010] crystal direction, the order parameter oscillates in the x direction. This oscillation corresponds to shifting of the Fermi surfaces oppositely along x, so that Cooper pairs form internally to each surface with wavevector $\Delta k\hat{x}$ (Fig. 3d). Since the real-space supercurrent density and the Josephson critical current can be regarded as Fourier conjugates[30], this pairing momentum results in finite weight of the interference at a particular magnitude of B_z that grows linearly with the parallel field, forming a 'V' shape. In our measurements of the device oriented with $\theta = \pi/2$, this splitting would be seen in the limit of strong BIA, but is not observed experimentally (Fig. 1e and Supplementary Information V). Additionally, when junctions are fabricated at an angle $\theta = \pi/4$, with strong BIA the behaviour is expected to shift from that shown in Fig. 3d to the nodal structure in Fig. 3b. Since we instead observe behaviour that does not depend on the crystal orientation, we conclude that BIA in our heterostructure is relatively weak. This conclusion agrees with a previous measurement of Shubnikov–de Haas oscillations in a HgTe quantum well, which was found to be consistent with strong SIA and weak BIA[31].

In the limit of overall weak spin–orbit coupling, the order parameter oscillates in both in-plane directions. Zeeman coupling at finite values of B_x leads to two concentric Fermi surfaces with opposite spin polarization, so that pairing occurs between surfaces with momentum in all in-plane directions (Fig. 3e). Increasing the parallel magnetic field causes the interference to both spread in B_z and periodically oscillate, a hybrid of the two above cases. Characteristically, at each node the two interference fringes adjacent to the central fringe combine to form the subsequent central fringe, a direct result of the inability to form nodes in the order parameter along lines of constant y. Although it is possible that this behaviour is present in the device with niobium leads, the nodal pattern is more consistent with strong SIA with aluminium leads at high density. In the limit of overall weak spin–orbit coupling, with the random phase χ the modelled interference successfully reproduces many aspects of the behaviour observed in the niobium device, but is still inconsistent with the aluminium devices (Fig. 3f).

As an additional study into the nature of electron pairing momentum, we explore the evolution of the minimum junction resistance at different parallel field B_x values, while energizing the global topgate to modify the bulk electron density. Devices used for these measurements were aligned such that $\theta = \pi/4$, corresponding to the devices of Fig. 1c,d,f–h. At the most positive gate voltage, as the magnetic field is increased the niobium device displays the

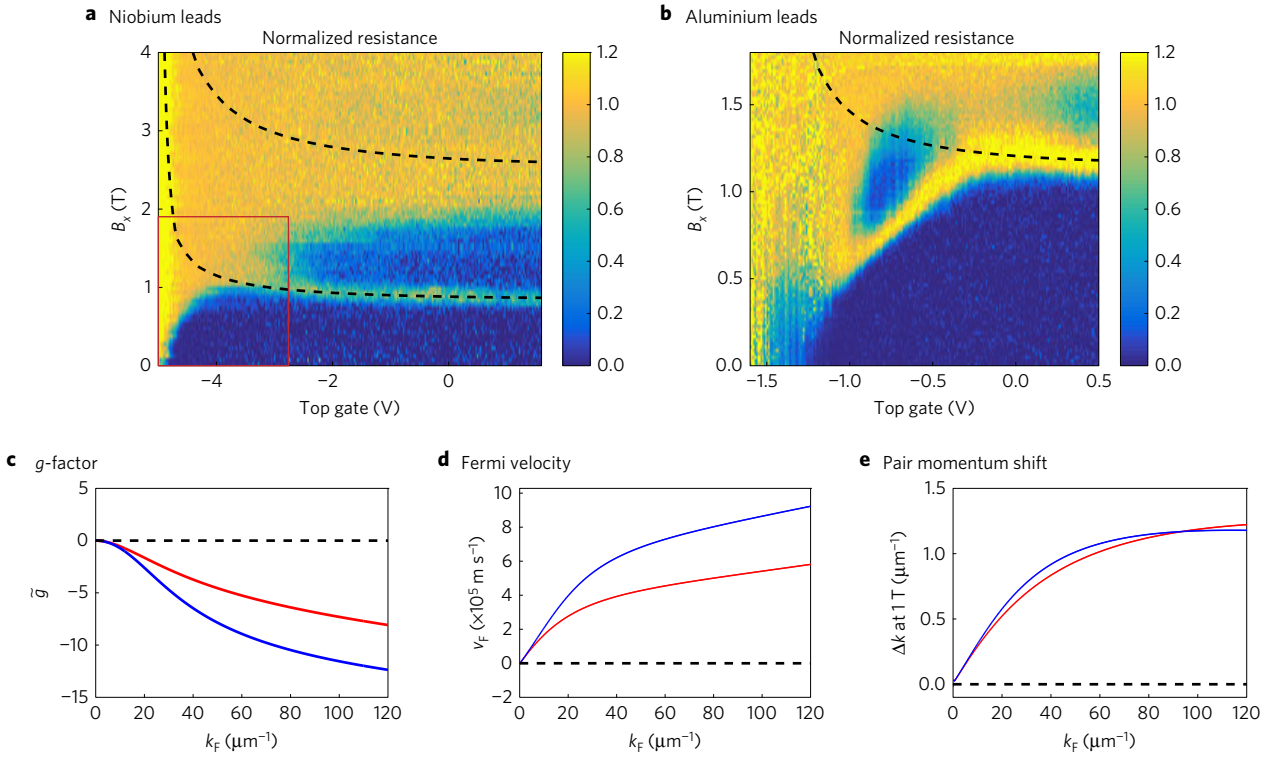

Figure 4 | The evolution of minimum differential resistance as density and parallel magnetic field B_x vary. Differential resistance measurements are normalized at each point by the normal junction resistance. **a**, At the highest gate voltage in the niobium junction, increasing the magnetic field leads to periodic high-resistance nodes separating regions of decreased resistance. As the gate voltage is decreased, the magnetic field at the first node rises to larger values of B_x. **b**, The aluminium junction behaves similarly to the niobium junction, although the measurement is limited to a smaller region outlined in red in **a**. At low density, the magnitude of the nodal magnetic field begins to decrease as the density is lowered, a feature that remains to be understood. **c**, The values of B_x at which we expect nodes to appear are sensitive to the density dependence of both the in-plane g-factors and the Fermi velocities, calculated here assuming that SIA is due to an electric field of 10 mV nm^{-1}. Blue and red curves correspond to the inner and outer Fermi surfaces, respectively. As the magnitude of the Fermi wavevector k_F decreases, the in-plane g-factors shift from −20.5 towards zero. **d**, Meanwhile the magnitudes of the Fermi velocities decrease to zero. **e**, The pairing momenta induced at 1 T consequently decrease to zero from approximately 1.2 μm^{-1}. Since there can be no induced momentum at zero density, the nodal magnetic field diverges as the density is lowered. The nodal magnetic field, averaged over the two Fermi surfaces, is calculated using BHZ theory and plotted as dashed black lines in **a** and **b**. The theoretical curves in **a** and **b** depend only on the parameters in **c**–**e**, and do not depend on the random phase χ.

node of increased resistance near $B_x = 0.9$ T (Fig. 4a). As before, an additional node is present near $B_x = 2.7$ T. When the topgate voltage is lowered to −5 V, the field magnitude of the lower node increases, first slowly and then more rapidly. In the device with aluminium leads, a similar nodal structure is observed, with the magnitude of the nodal field weakly increasing as the topgate voltage is lowered from 0.5 V to 0 V (Fig. 4b). Due to a doping layer in the heterostructure of the niobium device, more negative gate voltage is required in this device to achieve depletion (see Supplementary Information I).

The dependence of the nodal field magnitude on density can be calculated within the framework of our model based on BHZ theory, here assuming the presence of SIA due to a perpendicular electric field equal to 10 mV nm^{-1} (Supplementary Information VI). Since the magnitude of the induced Cooper pair momentum is approximately $\hbar\Delta k \approx \tilde{g}\mu_B B_x/v_F$, the dependence of both $\tilde{g}$ and v_F on the electron density will directly influence the magnitude of the parallel field needed to satisfy the nodal condition $\Delta kW = (2n+1)\pi/2$. Due to the inverted nature of the bands, the g-factors in the conduction bands are expected to evolve from −20.5 toward zero as the Fermi wavevector decreases[27], while the expected magnitudes of the Fermi velocities first decrease slightly and then more rapidly fall to zero (Fig. 4c,d). With these considerations we expect the magnitudes of the induced pairing wavevectors at 1 T to fall to zero from values near 1.2/μm as the Fermi wavevector decreases (Fig. 4e). As a result, the magnetic field needed to satisfy the nodal condition increases as the electron density decreases, finally diverging at zero electron density (calculated in black dashed lines in Fig. 4a,b). Although the overall evolution agrees well with the expectation from BHZ theory, we find that our measurements on niobium and aluminium devices respectively yield values of $\tilde{g}/v_F$ that are approximately 1.9 and 1.4 times greater than those expected theoretically (see Supplementary Information VI).

Several aspects of the density-dependent data do not fall into the modelling framework discussed above, and are interesting for further consideration. First, we expect that the position of the node associated with induced Cooper pair momentum should occur at higher parallel magnetic field as the density is reduced, a behaviour that we observe only at high density. As the density is further reduced, the magnitude of the nodal field eventually begins to decrease, an element of our model that is not present and remains to be understood, but could possibly be explained by a finite g-factor at zero density. Second, in the aluminium device, the region of reduced resistance occurring above the first node appears to be strongest near topgate voltages equal to −0.9 V and 0.5 V. We observe that these two regions of reduced resistance are connected by a region in which the resistance is more weakly reduced, but we have no reason to expect that the reduction in resistance above the first node should vary as the density decreases.

Our measurements demonstrate that a parallel magnetic field can be used both to tune the momentum of Cooper pairs in a material

and to clarify the nature of spin–orbit coupling in that material. A major current goal of condensed matter physics is to understand the nature of the superconductivity that results when electron pairing is combined with materials possessing exotic spin textures. Therefore, our new understanding that the superconducting order parameter can be engineered in space may be utilized to investigate spin physics within a broad range of materials including InAs-based quantum wells or the surfaces of three-dimensional topological insulators. Our method to tune the Josephson energy could find additional application in the field of quantum information processing, where direct control of the energy levels in a single superconducting qubit could provide a powerful tool for the investigation and optimization of qubit coherence. Finally, controlled evolution from singlet to triplet pairing could be used to probe the nature of pairing in superconducting materials, for example in devices similar to ours in which one of the *s*-wave leads is replaced by a superconductor with unconventional pairing.

Data availability

The data that support the plots within this paper and other findings of this study are available from the corresponding author on request.

Received 12 April 2016; accepted 3 August 2016; published online 19 September 2016

References

1. Meissner, W. & Ochsenfeld, R. Ein neuer Effekt bei Eintritt der Supraleitfahigkeit. *Naturwissenschaften* **21,** 787–788 (1933).
2. Bardeen, J., Cooper, L. N. & Schrieffer, J. R. Theory of superconductivity. *Phys. Rev.* **108,** 1175–1204 (1957).
3. Fulde, P. & Ferrell, R. A. Superconductivity in a strong spin-exchange field. *Phys. Rev.* **135,** A550–A564 (1964).
4. Larkin, A. I. & Ovchinnikov, Y. N. Inhomogeneous state of superconductors. *Sov. Phys. JETP* **20,** 762–769 (1965).
5. Kenzelmann, M. *et al*. Coupled superconducting and magnetic order in $CeCoIn_5$. *Science* **321,** 1652–1654 (2008).
6. Mayaffre, H. *et al*. Evidence of Andreev bound states as a hallmark of the FFLO phase in κ-$(BEDT\text{-}TTF)_2Cu(NCS)_2$. *Nat. Phys.* **10,** 928–932 (2014).
7. Predrag Nikolic, T. D. & Tesanovic, Z. Fractional topological insulators of Cooper pairs induced by the proximity effect. *Phys. Rev. Lett.* **110,** 176804 (2013).
8. Reeg, C. R. & Maslov, D. L. Proximity-induced triplet superconductivity in Rashba materials. *Phys. Rev. B* **92,** 134512 (2015).
9. Fu, L. & Kane, C. L. Superconducting proximity effect and Majorana fermions at the surface of a topological insulator. *Phys. Rev. Lett.* **100,** 096407 (2008).
10. Sau, J. D., Lutchyn, R. M., Tewari, S. & Sarma, S. D. Generic new platform for topological quantum computation using semiconductor heterostructures. *Phys. Rev. Lett.* **104,** 040502 (2010).
11. Yokoyama, T., Eto, M. & Nazarov, Y. V. Anomalous Josephson effect induced by spin-orbit interaction and Zeeman effect in semiconductor nanowires. *Phys. Rev. B* **89,** 195407 (2014).
12. Dolcini, F., Houzet, M. & Meyer, J. S. Topological Josephson ϕ_0 junctions. *Phys. Rev. B* **92,** 035428 (2015).
13. Buzdin, A. I., Bulaevskii, L. N. & Panyukov, S. V. Critical-current oscillations as a function of the exchange field and thickness of the ferromagnetic metal (F) in an S-F-S Josephson junction. *Pis'ma Zh. Eksp. Teor. Fiz.* **35,** 147–148 (1982).
14. Demler, E. A., Arnold, G. B. & Beasley, M. R. Superconducting proximity effects in magnetic metals. *Phys. Rev. B* **55,** 15174–15182 (1997).
15. Ryazanov, V. V. *et al*. Coupling of two superconductors through a ferromagnet: evidence for a π junction. *Phys. Rev. Lett.* **86,** 2427–2430 (2001).
16. Kontos, T. *et al*. Josephson junction through a thin ferromagnetic layer: negative coupling. *Phys. Rev. Lett.* **89,** 137007 (2002).
17. Sellier, H. *et al*. Temperature-induced crossover between 0 and π states in S/F/S junctions. *Phys. Rev. B* **68,** 054531 (2003).
18. Frolov, S. M. *et al*. Measurement of the current-phase relation of superconductor/ ferromagnet/superconductor π Josephson junctions. *Phys. Rev. B* **70,** 144505 (2004).
19. Oostinga, J. B. *et al*. Josephson supercurrent through the topological surface states of strained bulk HgTe. *Phys. Rev. X* **3,** 021007 (2013).
20. Meservey, R. & Tedrow, P. M. Properties of very thin aluminum films. *J. Appl. Phys.* **42,** 51–53 (1971).
21. Tinkham, M. *Introduction to Superconductivity* (Dover Publications, 2004).
22. Konig, M. *et al*. Quantum spin Hall insulator state in HgTe quantum wells. *Science* **318,** 766–770 (2007).
23. Hart, S. *et al*. Induced superconductivity in the quantum spin Hall edge. *Nat. Phys.* **10,** 638–643 (2014).
24. Bernevig, B. A., Hughes, T. L. & Zhang, S.-C. Quantum spin Hall effect and topological phase transition in HgTe quantum wells. *Science* **314,** 1757–1761 (2006).
25. Rothe, D. G. *et al*. Fingerprint of different spin-orbit terms for spin transport in HgTe quantum wells. *New J. Phys.* **12,** 065012 (2010).
26. Weithofer, L. & Recher, P. Chiral Majorana edge states in HgTe quantum wells. *New J. Phys.* **15,** 085008 (2013).
27. Konig, M. *et al*. The quantum spin Hall effect: theory and experiment. *J. Phys. Soc. Jpn* **77,** 031007 (2008).
28. Bychkov, Y. A. & Rashba, E. I. Properties of a 2D electron gas with lifted spectral degeneracy. *Pis'ma Zh. Eksp. Teor. Fiz.* **39,** 66–69 (1984).
29. Dresselhaus, G. Spin-orbit coupling effects in zinc blende structures. *Phys. Rev.* **100,** 580–586 (1955).
30. Dynes, R. C. & Fulton, T. A. Supercurrent density distribution in Josephson junctions. *Phys. Rev. B* **3,** 3015–3023 (1971).
31. Gui, Y. S. *et al*. Giant spin-orbit splitting in a HgTe quantum well. *Phys. Rev. B* **70,** 115328 (2004).

Acknowledgements

We acknowledge E. M. Hankiewicz and G. Tkachov for theoretical discussions. This work was supported by the NSF DMR-1206016, by the STC Center for Integrated Quantum Materials under NSF Grant No. DMR-1231319, by the NSF GRFP under Grant DGE1144152, and by Microsoft Corporation Project Q. We acknowledge additional financial support from the German Research Foundation (The Leibniz Program, Sonderforschungsbereich 1170 'Tocotronics' and Schwerpunktprogramm 1666), the EU ERC-AG program (Project 3-TOP) and the Elitenetzwerk Bayern IDK 'Topologische Isolatoren'.

Author contributions

The experiment is a collaboration between the Harvard and Würzburg experimental groups. S.H., H.R., M.K., G.B.-S., B.I.H. and A.Y. carried out the theoretical modelling and analysis.

Additional information

Supplementary information is available in the online version of the paper. Reprints and permissions information is available online at www.nature.com/reprints. Correspondence and requests for materials should be addressed to A.Y.

Competing financial interests

The authors declare no competing financial interests.